Proceedings of the Combustion Institute, Volume 28, 2000/pp. 1103–1109

STRUCTURE OF CRYOGENIC FLAMES AT ELEVATED PRESSURES

M. JUNIPER, A. TRIPATHI, P. SCOUFLAIRE, J-C. ROLON AND S. CANDEL
Laboratoire EM2C
Ecole Centrale de Paris
92295, Châtenay-Malabry, Cedex, France

This paper presents new experimental results on cryogenic jet flames formed by a coaxial injector at a pressure of 70 bar, which approaches the pressures found in rocket engines. This element, fed with liquid oxygen and gaseous hydrogen, is placed in a square combustion chamber equipped with quartz windows. The flame is examined via spectroscopy, OH* emission, and backlighting, the aim being to provide basic information on the flame structure. It is found that some of the OH* emission is absorbed by the OH radicals present in the flame. A detailed examination of this effect is presented, in which it is shown that, for this turbulent flame, the Abel transform gives the position of the intense reaction region, whether or not absorption is signficant. The flame is attached to the oxygen injector, as at low pressure. At high pressure, flame expansion is reduced compared with low pressure and is also less dependent on the momentum flux ratio between the hydrogen and the oxygen streams. An analysis of the relevant Damköhler numbers suggests that this is because the rate of combustion is mainly controlled by large-scale turbulent mixing at high pressure, and it is dominated by jet break-up, atomization, and vaporization at low pressures. Jet break-up is particularly dependent on the momentum flux ratio. Finally, the mean volumetric heat release rates and flame surface density in the experimental facility are estimated.

Introduction

The primary application of liquid oxygen (LOx)/gaseous hydrogen coaxial jet flames is in high-performance rocket motors, such as the Space Shuttle main engine and the Vulcain motor of Ariane 5. In each of the several hundred injectors, an annulus of high-velocity hydrogen provides the energy for rupture and turbulent mixing of a central oxygen jet. The propellants burn in a sheet around the atomized oxygen cloud. Typical chamber pressures of between 60 and 200 bar exceed the critical pressure of oxygen at 50.5 bar. Cryogenic flames operating at such elevated pressures differ from conventional spray flames, but only a limited number of studies in the literature relate to such flames. The objective of this investigation is to provide basic information on the flame structure as part of a large-scale research project into cryogenic combustion.

Our previous work on cryogenic flames concerned pressures up to 10 bar. A large set of images has been collected via laser elastic scattering from the oxygen jet, laser-induced fluorescence (LIF) of OH radicals, natural emission of OH* radicals, and backlighting [1–4]. This work was extended here to 70 bar, although laser techniques were not attempted, since excessive diffusion of the laser sheet and large collisional quenching effects were anticipated. The present analysis relied on OH* emission images combined with visualizations of the liquid oxygen jet. In scaling the injection conditions to different pressures, the momentum flux ratio of the two flows was conserved. This is defined as $J = \rho_{H_2} U_{H_2}^2 / \rho_{LOx} U_{LOx}^2$ and is an important factor in jet breakup [5]. To avoid excessive change in the mixture ratio $E = \dot{m}_{LOx}/\dot{m}_{H_2}$, the diameter of the hydrogen annulus was slightly reduced. In this article, the flame and oxygen jet shapes are compared with those obtained at low pressure for the same two values of the momentum flux ratio. While Refs. [6] and [7] already provide some data on high-pressure cryogenic flames, these results are the first published in which the pressure, oxygen jet dimension, and momentum flux ratio approach those of actual rocket motors.

Experimental Facility

The experimental facility, developed and operated by ONERA, was described in detail in Ref. [8] for low-pressure studies and Ref. [9] for high pressure. Oxygen at 80 K and hydrogen at 280 K were injected coaxially into a combustion chamber of height and width $10 \times d_{LOx}$ and length $100 \times d_{LOx}$. A visualization module, with windows of length $14 \times d_{LOx}$, can be placed at any point along the length of the chamber. In this study, two positions were used: 0 to $14 \times d_{LOx}$ and 8 to $22 \times d_{LOx}$. Injection conditions are presented in Table 1 for our experiments between 5 and 70 bar.

Imaging Techniques

The emission spectrum of a slice of the flame was recorded between 300 and 680 nm by a grating spectrometer with resolution $\Delta\lambda = 0.15$ nm and exposure time $r_{exp} = 1$ s. The slice was perpendicular to

TABLE 1
Operating Conditions under Investigation

Pressure	5 bar		10 bar		70 bar	
Re_{LOx}	67000		67000		134000	
J	14.4	6.5	14.5	6.5	11	6
E	3.0	4.5	2.1	3.2	1.6	2.2
V_{LOx} (ms^{-1})	2.2	2.2	2.2	2.2	4.0	4.0
d_{H_2}/d_{LOx}	2.4	2.4	2.4	2.4	2.0	2.0
V_{H_2} (ms^{-1})	432	292	308	207	190	150

J is the momentum flux ratio: $\rho_{H_2}U_{H_2}^2/\rho_{LOx}U_{LOx}^2$ and E is the mass flow ratio: $\dot{m}_{LOx}/\dot{m}_{H_2}$.

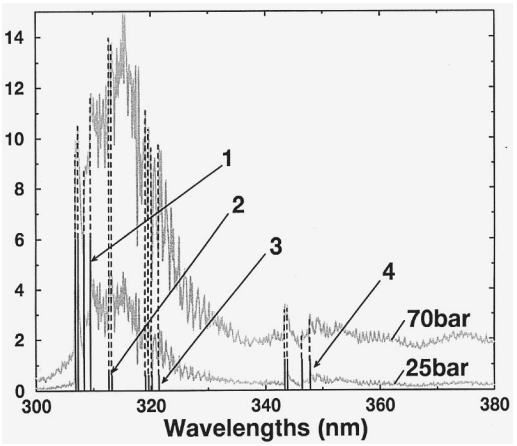

FIG. 1. Emission spectra of the flame at 25 and 70 bar. The theoretical positions of the band heads are marked in solid lines: 1 = band (0,0); 2 = band (1,1), 3 = band (2,2), and 4 = band (0,1). The extension of band heads to the intensities measured experimentally are marked in dotted lines.

the axis of the flame, 1 mm thick and located 30 mm from the injection plane. Only the part of the spectrum between 300 and 380 nm is shown here. This near-UV region corresponds to the emission of the OH* radical.

Spontaneous emission of the OH* radical was viewed at 6 Hz with an intensified charge-coupled device (CCD) camera with resolution 512 × 270 pixels. Two exposure times were used: 50 ns, to visualize instantaneous phenomena; and 3760 μs, to ensure smooth averaged images. These images were treated by the Abel inversion, a process whose validity is discussed later.

The camera was then synchronized with a spark flashlamp, placed at the focal point of a lens behind the chamber. Absorption by liquid oxygen, which occurred between 327 and 330 nm, was weak. However, light was scattered by the strong refractive index gradients at the edge of the jet. At the surface of supercritical oxygen, the density changed from 1100 kg m^{-3} to 100 kg m^{-3} in somewhat less than 1 mm [10]. The light deviation angle was estimated as $\theta = \partial n/\partial y = k\partial\rho/\partial y \approx 10°$ (from Gladstone's law, where $k = 2 \times 10^{-4}$ kg^{-1} m^3 for oxygen at atmospheric conditions). In the backlighting images, most or all of the light passing through the jet did not reach the camera, which collected light from the flashlamp with deviation less than 3°, so the jet appeared dark. Additionally, near the critical point, appreciable density fluctuations of the same scale as the wavelength of light gave rise to critical opalescence. The critical pressure of a mixture of O_2 with H_2 or H_2O is greater than the critical pressure of pure O_2, at 50.5 bar, so it is possible that parts of the jet were opalescent at 70 bar. This had the same net effect as light being scattered by the dense oxygen jet. By applying a threshold to eliminate the weaker refractive index gradients which were visible in the gas, the position of the jet was found. The average of all images gives the average time that the jet was present along the line of sight, and, thus, an idea of the rate of oxygen jet expansion.

The oxygen jet shielded emission from the rear portion of the flame while also scattering some light from other parts of the flame toward the camera. Its effect was limited to the central portion of the Abel inversion, corresponding to the predominant position of the jet. There was little or no flame surface there, and instead we concentrated on the more relevant outer regions of the flame. In summary, neither critical opalescence nor scattering from the jet interfered with the relevant parts of the Abel inversion.

Results

Flame spectra were obtained at pressures of 25 and 70 bar (Fig. 1). The filter used in the emission images isolates the bands of the $A^2\Sigma^+ \rightarrow X^2\Pi$ electronic transition of the 306.4 nm OH system. From 330 nm onward, the O_2 Schumann-Runge system and a continuous background are detected. This background comes most probably from ionization and ion recombination processes [11]. However, it is sufficiently weak to be neglected in the emission images. As expected, the global intensity of the flame increases with increasing pressure. Moreover, the relative intensities of the bands with respect to each other change. The (0,1) band becomes the strongest in the transition, instead of the (0,0) band.

Figure 2 shows instantaneous images ($\tau_{exp} \leq 50$ ns) of the flame and the jet and an averaged image of the flame. The instantaneous images are highly turbulent, but the average image is symmetric about the axis, leading one to assume axisymmetry of the mean flame structure. Already, much can be deduced from these images. They can also be treated further if the effect of absorption by species in the flame is considered.

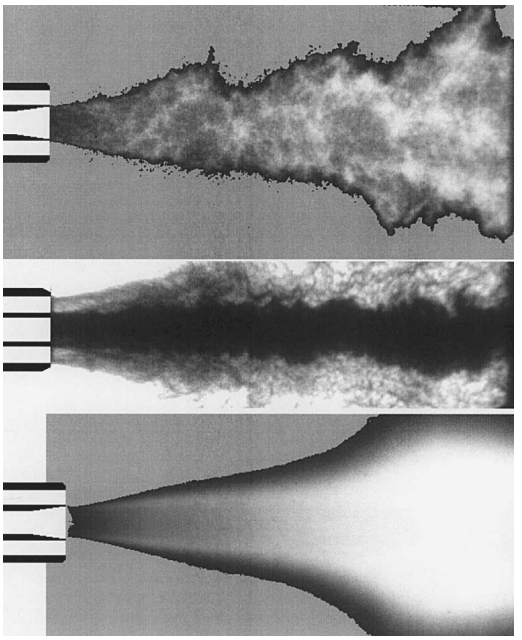

FIG. 2. Top: Instantaneous OH* emission image, $\tau_{exp} = 50$ ns. Middle: Instantaneous backlighting image, $\tau_{exp} < 50$ ns. Bottom: Average image of OH* emission, compiled from 30 images with exposure time 3760 μs.

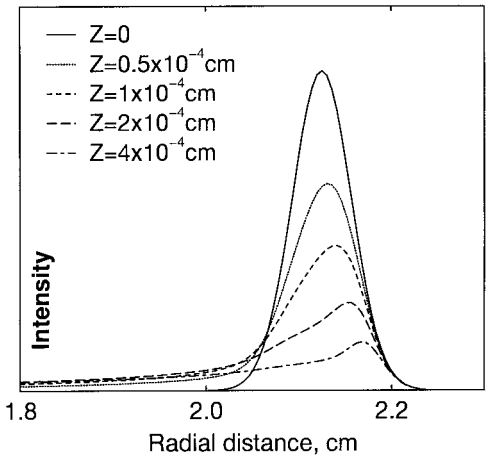

FIG. 3. Emission profiles calculated via the Abel inversion of a flame with various degrees of self-absorption, which is quantified by Z. As absorption increases, the apparent radius of maximum intensity increases, as does the apparent intensity in the central region.

Of the predominant species in the chamber (H_2, O_2, H_2O, and OH), only LOx and OH absorbed within the range 300–380 nm [12,13]. Absorption by LOx was limited to the jet and has already been discussed. To estimate the absorption by OH radicals, the Bouguer-Lambert relation was used: $I/I_0 = \exp(-k_\lambda p \int_l X_{OH} dl)$, where $k_\lambda(\lambda)$ is the OH absorption coefficient, p is the pressure, X_{OH} is the molar fraction of ground state OH, and l is the path length. Ref. [13] gives $k_\lambda(\lambda)$ for the (0,0) band of the A–X system of OH (at 306 nm), derived from shock-tube experiments for a mixture of $H_2/O_2/Ar$ at 60 bar and 1735 K. The highest k_λ, occurring at 306.47 nm, was 20 $atm^{-1}\,cm^{-1}$.

Absorption in the burned gases can be neglected, with $X_{OH} = 3 \times 10^{-5}$ (value at equilibrium calculated via CHEMKIN) and l equal to the size of the chamber, $I/I_0 = 90\%$. However, in the flame front, X_{OH} is much higher. The OH profile, which depends on the strain rate and pressure, is not known precisely at 70 bar for H_2/O_2 at high strain rates. For this reason, it was varied in the following simulations, each being characterized by $Z = \int X_{OH} dl$ across the entire flame front, even though only emission from the back of the flame has this optical path length.

Each simulation calculated the image that a camera would see when viewing a thin cylindrical self-absorbing flame from the side. The signal $S(y)$ was calculated via equation 1, where y is the vertical distance from the centerline, R is the outer radius of the flame, η_{opt} is the optical efficiency of the apparatus, $i_0(x, y)$ is the emission intensity, and $X_{OH}(x, y)$ is the mass fraction of absorbing species at position (x, y).

$$S(y) = \eta_{opt} \int_{-\sqrt{R^2-y^2}}^{+\sqrt{R^2-y^2}} i_0(x,y) \exp\left(-\int_x^{+\sqrt{R^2-y^2}} k_\lambda p X_{OH}(x',y) dx' \right) dx \quad (1)$$

The emission and X_{OH} profiles were assumed to follow the same Gaussian distribution. For ease of demonstration, the flame thickness and emission intensity were held constant while the maximum X_{OH} value changed for each simulation, thus simulating different values of Z. Then the Abel inversion of this image was calculated. With zero absorption, this was identical to the radial emission profile. Results with absorption are shown in Fig. 3. As absorption increases, the apparent flame position shifts to a larger radius. This is because, with appreciable absorption, the camera only sees the outer edge of the nearest half of the flame. The resulting image is similar to half the full axisymmetric distribution but with the flame shifted outward, which is reflected in the Abel inversion. Also, the apparent intensity of the central portion rises slightly because the absorption path

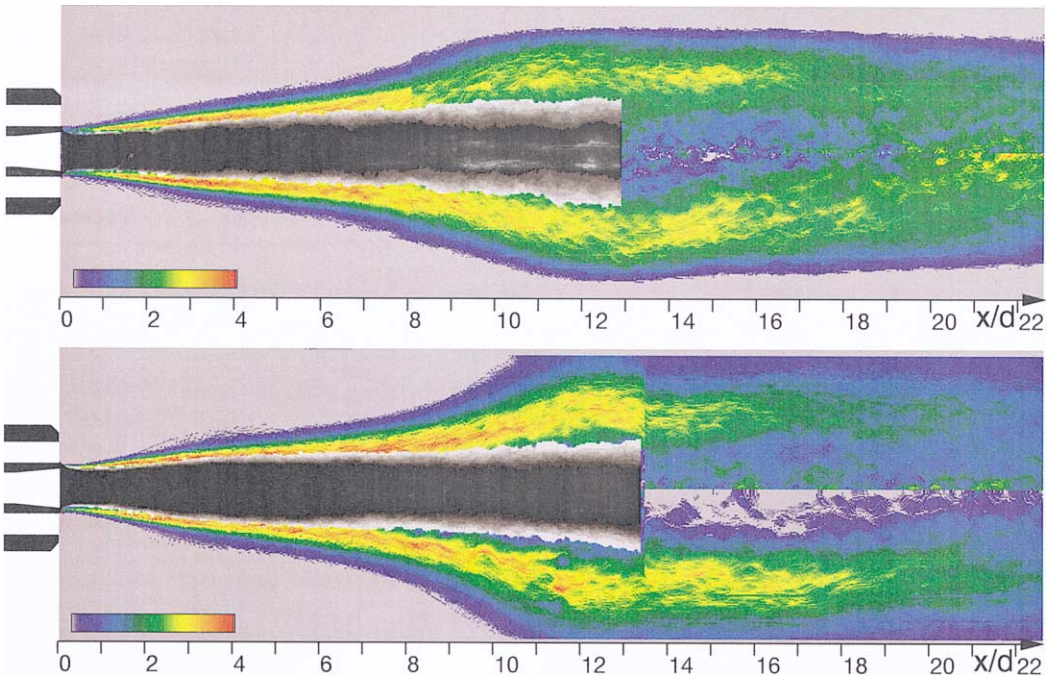

FIG. 4. Top: $J \approx 11$. Bottom: $J \approx 6$. Color levels (adjusted to obtain the maximum range): Abel transform of the time-averaged natural OH* emission images at 70 bar. The top and bottom halves of each image are processed separately, so they do not match at the axis, where the inversion is particularly sensitive to error. Gray levels: Average time that the jet was present along the line of sight, from 100% in black to 25% of the time in light gray. Jet position data were available only in the region 0 to $12 \times d_{\mathrm{LOx}}$.

length is greater at the top and bottom of the circular flame than at the center.

A cross section of the turbulent cryogenic flame can be considered as a circle with a wrinkled circumference. The flame is much thinner than the distance over which its radial position fluctuates. Even if the camera only sees the outer layer of the flame, on average the effect of this displacement is negligible compared with the effect of the turbulent fluctuation. Thus, the position of maximum intensity on the Abel-inverted average image will be the same with or without absorption. However, it will still be the case that the absorption path length is, on average, higher at the top and bottom of the flame than in the middle. Therefore, the Abel inversion on the averaged images will yield higher intensities in the central region than are actually present in the radial intensity profile.

Figure 4 shows the Abel-transformed average emission images with the average jet position superimposed. The images vary little between different values of the momentum flux ratio. To provide more detail on flame stabilization, the optical apparatus was zoomed on the near-injector region (Fig. 5).

The average jet position expanded from the injector at a constant angle of around 3°. The flame was attached to the oxygen tube lip, although the time-averaged intensity here was low. Between $1 \times d_{\mathrm{LOx}}$ and $7 \times d_{\mathrm{LOx}}$, the time-averaged intensity increased rapidly and passed a maximum between 2 and $4 \times d_{\mathrm{LOx}}$. The width of the time-averaged reacting region, which lies just outside the jet, also increased. At $7 \times d_{\mathrm{LOx}}$, the reacting region thickened and bloomed away from the jet. The total intensity at a given cross section increased to a maximum at $12 \times d_{\mathrm{LOx}}$. After $12 \times d_{\mathrm{LOx}}$, the reacting region was thick, but extended to smaller and smaller radii, so the total intensity at a given cross section decreased. Little can be inferred from the data in the central region since the error in the Abel transform was at its greatest.

Effect of Pressure

At low pressures, ligaments and droplets existed at the edge of the jet. These were no longer evident at 70 bar (Fig. 2), where the dense oxygen was in the form of packets with indistinct edges, similar to the observation in Ref. [7]. The spectrum shows that the global intensity of the flame increases by a factor 3.5 when the pressure changes from 26 to 70 bar. Low-pressure images can be found in Refs. [1–4].

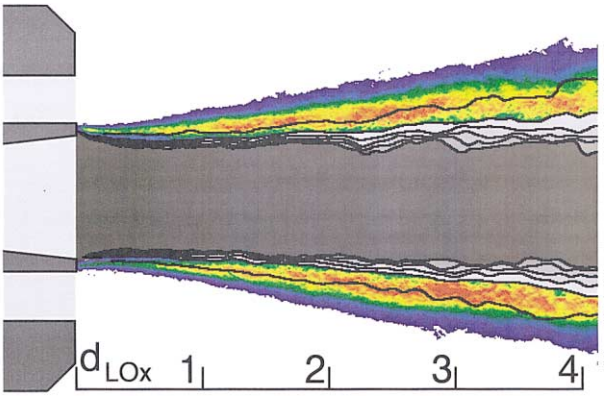

FIG. 5. Color levels: Abel transform of the time-averaged natural OH* emission images at 70 bar. In black: Contours of the averaged jet position. In the central gray region, the jet is present along the line of sight all the time, at the next contour seven-eighths of the time and at the outer contour, which lies within the time-averaged reaction zone, one-eighth of the time.

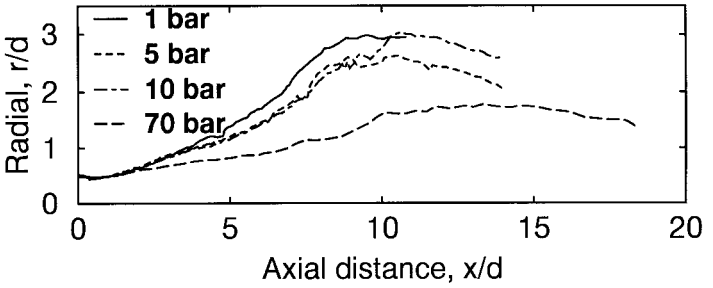

FIG. 6. Position of the maximum intensity of the Abel-transformed images for cryogenic flames at different pressures but similar momentum ratios (J = 14.5 at 1, 5, and 10 bar, J = 11 at 70 bar). At 70 bar, the hydrogen tube is 2 × d_{LOx} diameter instead of the 2.4 × d_{LOx} at lower pressures.

At low pressures, the time-averaged emission intensity was greatest at the oxygen injector lip, whereas at 70 bar, it was greatest at 2–4 × d_{LOx}. A useful indication of average flame shape is the position of the maximum time-averaged emission intensity, which is shown in Fig. 6. At low pressures, the flame follows the surface of the cylindrical liquid jet for 1–2 × d_{LOx} before blooming out rapidly. At 70 bar, with a smaller hydrogen tube diameter, the flame expands progressively but slowly up to 7 × d_{LOx} where it blooms slightly.

Effect of Momentum Flux Ratio

According to Ref. [5], the momentum flux ratio, J, is an important factor controlling jet breakup, since a well-dispersed liquid phase aids rapid vaporization. However, the results of Ref. [1] for a coaxial cryogenic flame showed that as the pressure increased, J had increasingly less effect on the flame shape, and this tendency was noted here at 70 bar. However, at high J, where hydrogen is more in excess, the flame extended to a marginally smaller radius after x/d = 12.

Discussion

In the cryogenic jet flame, oxygen must first evaporate, then be transferred to the flame front by large-scale turbulent structures, where it burns. The mechanisms involved are complex, and, rather than consider these in detail, a comparison of characteristic times is proposed in order to highlight the general tendencies. These characteristic times are the vaporization time τ_v, the large-scale mixing time $\tau_m = L/(U_g - U_l)$, and the chemical time $\tau_c = D_{O_2}/s_l^2$. L is a characteristic distance, D_{O_2} the diffusivity, and s_l the laminar flame speed.

Ref. [3] showed that the chemical Damköhler number, $Da_c = \tau_m/\tau_c$ is typically between 10 and 100 at 1 to 10 bar, which we confirmed at 70 bar. Thus, the chemical reaction rate is not a limiting factor. The vaporization Damköhler number, $Da_v = \tau_m/\tau_v$, compares the large-scale turbulent mixing time with the vaporization time. At subcritical pressures, τ_v can be estimated via the model of an isolated droplet in a gas at rest: $\tau_v = d^2\rho_l/[8D_{O_2}\rho_g \ln(1 + B)]$. The droplet size, d, is typically 10 to 80 μm. The ambient gas is taken to be water vapour at 1000 K. The Spalding transfer number, $B = C_p(T_g - T_{Lox})/L_v$ = 10. Thus, at 1 to 10 bar, Da_v is between 0.01 and 2, meaning that evaporation is the slowest and therefore dominant mechanism. At 50 bar, Da_v is between 0.1 and 14, which is less conclusive. However, around and above the critical pressure, surface tension diminishes. As a result, Delpanque and Sirignano [14,15] proposed that aerodynamic instabilities on the surface of a droplet are undamped and grow rapidly. Consequently, the outer layer of the liquid strips off and mixes with the surrounding gas

in a gasification process analogous to vaporization, dependent also on small-scale turbulent structures. According to their numerical simulations, the gasification rate is larger than the vaporization rate at the same pressure by at least an order of magnitude. This brings the new gasification Damköhler number, Da_g, to between 1 and 140. Furthermore, the Reynolds number increases with pressure leading to faster small-scale mixing. These two effects combine to suggest that large-scale turbulent mixing becomes the slowest and therefore most influential parameter when the pressure is higher than the critical pressure of the liquid.

The rate of large-scale turbulent mixing is proportional to the relative velocity of the two fluids. To retain the same momentum flux ratio at high pressure, this relative velocity was reduced in our experiments, diminishing the turbulent mixing. This may explain why the flame expanded less at high pressure. We can now explain why the flame was less sensitive to the momentum flux ratio at higher pressure: The momentum flux ratio affected jet breakup, which affected vaporization. However, at 70 bar the flame was in a regime limited by the subsequent mixing of the gases rather than by vaporization and jet breakup.

It was possible to obtain some first-order estimates of the mean volumetric heat release rate and the flame surface density. The oxygen mass flow rate was 0.05 kg s^{-1} at 10 bar and 0.10 kg s^{-1} at 70 bar. The volume containing the flame surface was estimated from the emission images to be 170 cm^3 at 10 bar and 100 cm^3 at 70 bar. Given that 15×10^6 J are released when 1 kg of oxygen combusts, the mean volumetric heat release can be estimated as 50×10^8 W m^{-3} at 10 bar and 150×10^8 W m^{-3} at 70 bar. To a first approximation, the consumption of oxygen per unit flame surface was that of a strained flame between streams of oxygen and hydrogen. Ref. [3] calculated the rate of oxygen consumption per unit flame surface at 1 bar to be approximately 1 kg m^{-2} s^{-1}. This quantity is proportional to $\rho\sqrt{D\dot{\varepsilon}_s}$, where D is the species diffusivity and $\dot{\varepsilon}_s$ is the strain rate, assumed to be proportional to the relative velocity of the two fluids. Mass diffusivities of oxygen in an oxygen/water vapor environment were calculated from the information gathered in Ref. [16]. The quantity $\rho\sqrt{D\dot{\varepsilon}_s}$, relative to that at 1 bar, was found to be 1.82 at 10 bar and 3.80 at 70 bar. This, combined with the mass flow rate and the volume occupied by the flame, gave an estimate of the flame surface density: 160 m^{-1} at 10 bar and 261 m^{-1} at 70 bar. In a real motor, the flame surface density may take even higher values due to close packing of the injectors.

Conclusions

The structure of a single cryogenic flame was examined at a pressure of 70 bar using spectroscopy, OH* emission, and backlighting. The aim was to provide basic information on the flame structure at conditions close to real rocket engines, above the critical pressure of oxygen at 50.5 bar.

Spectra in the visible region indicated strong OH* emission. The relative intensities of emission bands changed, and the global intensity increased with pressure. Backlighting images showed that, at high pressure, the jet had an indistinct edge and broke up into packets, whereas at low pressure, ligaments and droplets were visible. Emission images of OH* showed that the flame was attached to the lip of the oxygen injector, although the intensity here relative to the rest of the flame was lower at 70 bar than at 1 to 10 bar. Scaling from low to high pressures was achieved by retaining the same value of J, the momentum ratio of the two fluids. The flame expanded less at high pressure, and this expansion was less dependent on the momentum ratio.

The effect of absorption of OH* emission by species present in the chamber was also investigated. The only significant absorption arose from OH radicals in the flame. Since the exact OH profile was not known, the effect was calculated over a range of profiles. It was shown that the Abel inverted average images gave the position of the intense region whether or not absorption was significant. However, under very high self-absorption, the central region may show artificially enhanced intensities.

Analysis indicated that the rate of combustion changed from being strongly dependent on the vaporization rate at low pressure to being dependent on the turbulent mixing rate at high pressure. The former was strongly influenced by jet breakup and J, whereas the latter was more dependent on the velocity of the hydrogen flow. This explains why J had less effect on the flame at high pressure.

Acknowledgments

This study was supported in part by SNECMA and CNES through the Groupement de Recherche "Combustion dans les moteurs fusées." The experimental facility was operated by L. Vingert of ONERA with the assistance of A. Mouthon and J. Champy.

REFERENCES

1. Herding, G., "Analyse expérimentale de la combustion d'ergols cryotechniques," Ph.D. thesis, École Centrale Paris, ECP 19, 1997.
2. Herding, G., Synder, R., Rolon, J., and Candel, S., *J. Prop. Power* 14:146 (1997).
3. Snyder, R., Herding, G., Rolon, J., and Candel, S., *Combust. Sci. Technol.* 124:331 (1997).
4. Tripathi, A., Juniper, M., Scouflaire, P., Rolon, J., Durox, D., and Candel, S., Thirty-Seventh AIAA Conference, Los Angeles, 1999.

5. Hopfinger, E., and Lasheras, J., in *Sixth International Conference on Liquid Atomisation, Spray Systems*, (A. J. Yule and C. Dumanchel, eds.), ICLASS, Begell House, New York, 1994; pp. 110–117.
6. Mayer, W., and Tamura, H., *J. Prop. Power* 12:1137 (1996).
7. Mayer, W., Shick, A., Vielle, B., Chauveau, C., Gokalp, I., Talley, D., and Woodward, R., *J. Prop. Power* 14:835 (1998).
8. Kendrick, D., Herding, G., Scouflaire, P., Rolon, C., and Candel, S., *Combust. Flame* 118:327 (1999).
9. Vingert, L., Habiballah, M., Hervat, P., Dugué, F., and Vuillermoz, P., in *Troisième Colloque Franco-Allemand sur la Combustion dans les Moteurs-Fusée*, Marseille, France, 1997.
10. Oefelein, J., and Yang, V., *J. Prop. Power* 14:843 (1998).
11. Gaydon, A., *The Spectroscopy of Flames, 2nd ed.*, Chapman and Hall, London, 1974.
12. Pearce, R., and Gaydon, A., *The Identification of Molecular Spectra, 3rd ed.*, Chapman and Hall, London, 1965.
13. Davidson, D., Roehnig, M., Petersen, E., Di Rosa, M., and Hanson, R., *J. Quant. Spectrosc. Radiat. Transfer* 55 (1996).
14. Delplanque, J.-P., and Sirignano, W., *Atomiz. Sprays* 4:325 (1994).
15. Delplanque, J.-P., and Sirignano, W., *Combust. Sci. Technol.* 105:327 (1995).
16. Oefelein, J., "Simulation and Analysis of Turbulent Multiphase Combustion Processes at High Pressures," Ph.D. thesis, Pennsylvania State University, University Park, PN, 1997.

COMMENTS

Josette Bellan, Jet Propulsion Laboratory, USA. I am intrigued by your identification of the excited OH radical regions with the flame under supercritical conditions. Under subcritical conditions, we know that the radical is very active in the flame; the elementary kinetic schemes show this. It is not obvious to me that the same situation exists under supercritical conditions; in particular, there are no equivalent kinetic schemes at high pressure. Therefore, I am wondering if you base your inference of identification of the flame with the excited OH radical upon established spectroscopic information, or if this inference is a mere extrapolation from the subcritical information.

Author's Reply. This question highlights the lack of work on high-pressure reaction mechanisms in the literature. However, we believe that there are two pieces of evidence which allow us to identify the flamefront with the excited OH radical. First, our spectra show that the predominant emission, both at ambient and at high pressure is in bands associated with this radical. Furthermore, our instantaneous images show that this emission is localized in a thin front. Second, at high pressure, the production rates and mole fraction profiles of an H_2/O_2 flame with complex chemistry have been calculated [1]. H, O, and OH are all localized around the flamefront. Due to the lack of other evidence, we have to extrapolate from reaction mechanism data at ambient pressure [2], which indicates that OH* is created only from H, O, and OH. Once created, OH* releases a photon typically within 1.5 μs or is de-excited by a collision. This is considerably shorter than typical convection or diffusion times in the chamber, allowing us to assume that OH* created within the flamefront will emit within the flamefront.

REFERENCES

1. Daou, J., Haldenwang, P., and Nicoli, C., *Combust. Flame* 101:153–169 (1995).
2. Dandy, D., and Vosen, S., *Combust. Sci. Technol.* 82:131–151 (1992).